International Journal of Hydrogen Energy 127 (2025) 38–50

Contents lists available at ScienceDirect

International Journal of Hydrogen Energy

journal homepage: www.elsevier.com/locate/he

Breaking limits of solar-to-hydrogen efficiency via synergy with batteries

Uchechi Chibuko [a,b,*], Tsvetelina Merdzhanova [a], Solomon Agbo [a,c], Uwe Rau [a,d], Ursula Wurstbauer [b], Oleksandr Astakhov [a]

[a] IMD3-Photovoltaics, Forschungszentrum Jülich GmbH, 52425 Jülich, Germany
[b] Department of Physics, University of Münster, 48149 Münster, Germany
[c] UE, Forschungszentrum Jülich GmbH, 52425 Jülich, Germany
[d] Jülich Aachen Research Alliance (JARA-Energy) and Faculty of Electrical Engineering and Information Technology, RWTH Aachen University, Schinkelstr. 2, 52062 Aachen, Germany

ARTICLE INFO

Handling Editor: Suleyman I. Allakhverdiev

ABSTRACT

Coupling of photovoltaics (PV) with electrochemical (EC) water splitting is an established concept for storage of excess PV energy via production of green hydrogen. However, intermittent PV output presents a challenge for the stability and lifetime of EC devices in both direct coupled and power electronic assisted systems. The use of batteries is a viable way of smoothing out PV output fluctuations, which is beneficial for EC stability and ultimately lifetime. In our studies of direct coupled PV-EC-battery (PV-EC-B) systems, we have demonstrated self-sustaining operation of the device without control electronics. In addition to the expected storage function, the batteries stabilize the power coupling and improve the solar-to-hydrogen (STH) efficiency of the system despite their own power losses. This synergistic effect originates from the distribution of the daily PV energy over longer periods of EC operation i.e. the reduction of the EC input power and the related kinetic losses. This STH efficiency gain is addressed from two orthogonal viewpoints. First, we investigate how high the synergistic STH gain can be in the optimized system composed of high-efficiency PV and EC components operating close to the system efficiency limit. We show that in a basic day-night operating cycle, an optimally coupled PV-EC system with STH efficiency of 23.0 % can reach STH efficiency of 25.4 % once battery is included. The STH efficiency increase achieved in the PV-EC-B system is 2.4 % abs. higher than the STH efficiency in the reference PV-EC system and 1.9 % abs. higher than the theoretical STH limit of the reference system determined by the EC polarization curve. The second aspect is related to the downscaling of an electrolyzer facilitated by the reduced EC power in the system with battery. We show that the battery allows a reduction of the electrolyzer capacity in the PV-EC-B system by about a factor of two, while operating at the same efficiency as the reference PV-EC system. These results are crucial for the future design, techno-economic and life cycle analysis of advanced PV-powered water splitting.

1. Introduction

Coupling photovoltaics (PV) and energy storage is a critical step in achieving a balanced renewable energy system across different timescales. Storage is of paramount importance in situations where the grid is either unavailable or weak [1]. However, significant penetration of photovoltaics necessitates the use of storage for virtually any grid [2]. The short-term storage issue is predominantly addressed by batteries [2–5] (B) and the long-term storage is expected to be addressed by the electrochemical (EC) reactors producing solar fuels, particularly hydrogen [6–10]. Combining EC cells with battery storage in a PV-EC-B hybrid system is a technically feasible approach to stabilize the PV power supply [6,11–13] while the battery price reduction trend [14] promises its economic viability. Stable baseload provided by batteries can improve safety [15] and stability [16] of water splitting especially in alkaline electrolyzers. This furthermore implies that batteries can provide the requisite potential difference to maintain the polarization and operational status of the EC cell [13,16], thereby preserving the catalytic activity of the electrodes and preventing degradation due to the intermittent nature of realistic irradiance [13]. Batteries and electrolyzers are typically connected to photovoltaics via power electronics, with multiple DC-AC-DC conversion of electric power in some cases [5,6,8,17–19].

* Corresponding author. IMD3-Photovoltaics, Forschungszentrum Jülich GmbH, 52425 Jülich, Germany.
E-mail address: u.chibuko@fz-juelich.de (U. Chibuko).

https://doi.org/10.1016/j.ijhydene.2025.04.166
Received 23 January 2025; Received in revised form 17 March 2025; Accepted 9 April 2025
Available online 11 April 2025

However, solutions that employ direct coupling of PVs to EC devices [18,20–28] or batteries [29–35] have also demonstrated the potential for efficient self-sustained operation and the highest solar-to-hydrogen efficiencies (STH) are typically attained in laboratory-scale direct--coupled systems [18,20–28]. Authors of a few papers point out that power electronics is not necessary when PV is coupled to battery [31, 36–40], and properly combined components allow efficient operation of PV-EC [20–22,26,41] or PV-B [29–34,42] systems under realistic variations in irradiance and PV-module temperature.

In our previous work, we have studied the interplay of PV, EC cell, and battery in the simplest direct-coupled PV-EC-B system and demonstrated its self-sustaining operation in idealized day/night operating cycles [43,44]. In the absence of power conditioning electronics, the battery facilitates power coupling in the system during the day and extends the operation of the EC device into the night which is commonly reported [45,46]. In addition to the expected stabilizing effects, we have found theoretically [43] and confirmed experimentally [44] that batteries can improve the solar-to-hydrogen (STH) efficiency in PV-EC-B systems compared to the PV-EC reference without battery. The STH gain is achieved as the battery transfers some part of the daytime energy to the night, extending the operating time and thus reducing the operating power of the electrolyzer and therefore kinetic overpotential loss in the EC device. The gain is synergistic - even with additional losses in the battery, the common losses in the EC-B combination are lower than in the EC cell operating alone. In a complete operating cycle of the PV-EC-B system, the electric charge supplied at the PV voltage during the day is completely used for water splitting at the end of the cycle, reaching the fixed reference potential of 1.23V. Therefore, as it has been discussed in detail in Ref. [43], regardless of the route taken by the current, the total potential loss is still the difference between the PV voltage and the reference potential (multiplied by the number of EC cells in series). That is, the inevitable potential loss in the battery reduces the operating voltage of the electrolyzer during the night, but does not increase the total potential loss [43,44]. This synergy between EC and battery in a simple direct-coupled PV-EC-B system motivates our further research in two main directions. The first is the stable round-the-clock hydrogen production with increased STH efficiency. We seek to determine how far the STH gain in the PV-EC-B system can be improved in a system with high efficiency components. The second aspect is related to the downscaling of the electrolyzer capacity achievable in the system with battery [46,47]. For the same PV size and target EC power density, a smaller electrolyzer is required in the system with battery, which is of interest considering that the electrolyzer represents 30 %–50 % of levelized cost of hydrogen [48–50].

In this work, we address both aspects in well-defined experiments with idealized day/night cycles, where the PV operates under constant irradiance during the “day” and is off during the “night”. This idealized operating cycle allows accurate measurement of the STH efficiency gain in the PV-EC-B system and provides a direct comparison with the reference PV-EC system measured under standard PV test conditions (AM1.5g). In the first experiment, we investigate how far the STH efficiency can be increased in the system of a high-efficiency GaAs concentrator PV module driving an industrially relevant water-splitting electrolyzer stack combined with a commercial lithium-titanium oxide battery pack. We compare the optimized PV-EC-B system to the optimized reference system driving the same electrolyzer with the same idealized PV power profile to isolate the effect of the battery and accurately determine the achieved STH gain. This reference PV-EC system after optimization operates very close to the theoretical STH limit determined by reverse analysis of the EC polarization curve [51]. Then, a PV device of the same area and efficiency is optimally coupled to the same electrolyzer, but with the battery connected in parallel. The system with battery demonstrates self-sustained operation in a day/-night cycle, it shows significant STH efficiency gain against the reference system, and notably reaches STH efficiency value above the theoretical STH efficiency limit of the reference PV-EC system. In the second set of experiments, we investigate the electrolyzer downscaling potential when coupled to a battery. The ratio of the PV area, A_{PV} to the EC area, A_{EC} has been adjusted such that the electrolyzer capacity per unit PV area in the PV-EC-B system was twice as small as in the reference PV-EC system while resulting in approximately same STH efficiency. After presenting the system design considerations and the experimental procedure, the results are presented in two logical blocks (i) the experiment breaking the STH limit and (ii) downscaling of the EC capacity relative to PV. The study shows useful synergy in common operation of the EC cells and battery, and is a starting point for advanced experiments with realistic PV generation profiles.

2. Methods

2.1. System design and power coupling

Schematic diagram of a PV-EC system is illustrated in Fig. 1(a) and of a PV-EC-B in Fig. 1 (b). An idealized duty cycle is presented in Fig. 1 (c) illustrating the difference in operation of both systems. The duty cycle consists of a light time (T_l) and dark time (T_d) shown with sun and moon symbols respectively. In the PV-EC system, the PV current (I_{PV}) is directly utilized in the water splitting reaction in the EC cell when there is sufficient irradiance, and the system is idle in the dark. For the PV-EC-B system, as shown Fig. 1 (c), the PV current I_{PV} during T_l is split between the EC cell and the battery. The EC cell current (I_{ECl}) is directly utilized for water splitting (with total charge (Q_{H2l}) and the battery current (I_{Bl}) accumulates in the battery to a charge (Q_B). During the dark time T_d the battery discharges through the EC device with current (I_{ECd}). This leads to the production of hydrogen in the absence of sunlight during T_d with a dark time charge (Q_{H2d}) obtained from the integration of the EC dark time current. For proper assessment of the STH efficiency in the PV-EC-B system it is essential to complete the cycle with utilization of the accumulated charge Q_B during the dark time so that $Q_B = Q_{H2d}$ [52]. This necessitates batteries with close to 100 % columbic efficiency, which is attainable with contemporary battery technologies, at least during initial operations [53,54]. The overall battery efficiency is determined by the product of its columbic/faradaic efficiency and its voltage/overpotential efficiency. Given that the total battery overpotential loss is subtracted from the EC overpotential loss during the night, as explained in the introduction, the effect of the battery losses are rendered inconsequential.

In both cases efficient system operation relies on the proper choice of elements’ *IV* characteristics for the utilization scenario. More specifically, for the case of the direct-coupled PV-EC system, the operating point or working point which is at the intersection of PV and EC *IV* characteristics must be as close as possible to the maximum power point of the PV device to utilize the full potential of the PV generator. The optimal coupling for the ideal system is formalized as

$$P_{EC} = P_{WP} = P_{MPP} \tag{1}$$

Where P_{EC} is the power delivered to the EC terminals or working point power P_{WP} and P_{MPP} is the maximum power delivered by the PV device. Giving the possibility of working below the P_{MPP} since PV and load/EC *IV* characteristics may not always intercept the PV’s P_{MPP} (i.e. non ideal conditions), the issues related to optimal coupling as well as the degree of the coupling are well described in numerous papers [18,20–22,24,26, 28,29,31–35,43,44,51]. The coupling factor C [33,34,43] or coupling efficiency η_C [18,34] is the ratio of the PV working point P_{WP} to the PV maximum power P_{MPP} as shown in equation (2).

$$C = \eta_C = P_{WP}/P_{MPP} \tag{2}$$

The first step towards maximizing the coupling efficiency η_C of the direct-coupled system is to define the power requirement of the load. It is common to address this issue graphically by plotting the current-voltage and power-voltage characteristics of PV and EC devices. Both

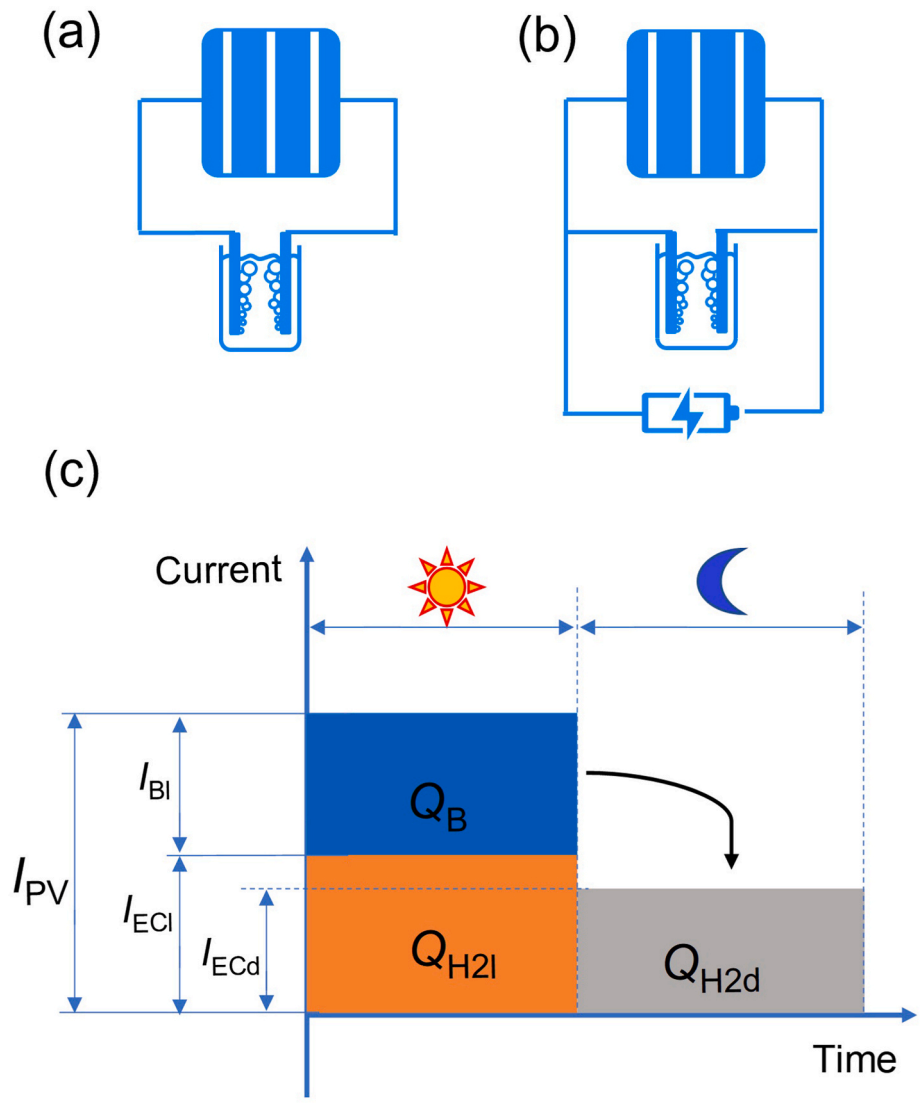

Fig. 1. (a) Schematic diagram of PV module direct coupling to electrochemical cell referred to as PV-EC. (b) Schematic diagram of PV module direct coupling to parallel connected electrochemical cell and battery referred to as PV-EC-B. (c) Illustration of duty cycle of PV-EC-B system showing current (*I*) and charge (*Q*) distributions over a light time and dark time shown with sun and moon symbols, respectively.

kinds of plots are employed in Fig. 2. First, we focus on the coupling and scaling of PV and EC devices. In this work, we start the system design from the electrolyzer. The characteristic power versus voltage plot for the electrolyzer is shown in Fig. 2 (a) with solid blue line. The electrolyzer is made up of a stack of 3 EC cells connected in series. Considering an industrial relevant working voltage of 1.8V per EC cell in the stack [55,56], the required stack voltage sums up to 5.4 V (V_{EC}) which corresponds to a power value of 14.3 W. Therefore, a PV with power of 14.3 W is required. This power requirement is shown with red line labeled as P_{WP} in Fig. 2 (a) which intercepts the EC power curve at 5.4 V shown with gray circle. After the target coupling power and voltage are determined, the respective target current can be determined by considering the current voltage characteristics of the elements. The EC polarization curve is plotted in Fig. 2 (b) with a solid blue line. The horizontal constant power line presented in Fig. 2 (a) turns to a reciprocal curve in Fig. 2 (b) representing all possible maximum power points of any PV device with $P_{MPP} = 14.3$ W. The intersection of this reciprocal line with the EC polarization curve gives the current and voltage coordinate for MPP of a PV device optimally coupled to the electrolyzer in question. Using the determined current and voltage of the target MPP we can select or adjust the PV device to ensure optimal coupling in the PV-EC system. The example of the required PV *IV* characteristic is shown with solid black line in Fig. 2 (b).

The required PV *IV* characteristic is a result of scaling and interconnecting the basic PV elements that are either cells or modules. The logic behind the adjustment is introduced in the following.

The current I_{PV} of a PV cell can be expressed via the cell current density J_{PV} as

$$I_{PV} = J_{PV}\, A_{PVcell}/\chi \tag{3}$$

where A_{PVcell} is the PV cell area and χ is the solar irradiance concentration ratio for the case of concentrator PV devices.

Considering the given single-cell PV module, with known efficiency, the next step is to define the area of the PV element required to generate the power requirement of the load. For the case with solar concentration, we define the PV area A_{PV} as the area of the solar concentrator/receiver/aperture ($A_{concentrator}$) as expressed in equation (4) [57],:

$$A_{PV} = A_{concentrator} = A_{PVcell}\cdot\chi \tag{4}$$

The required PV device area for a given EC power requirement can therefore be calculated using the following equation:

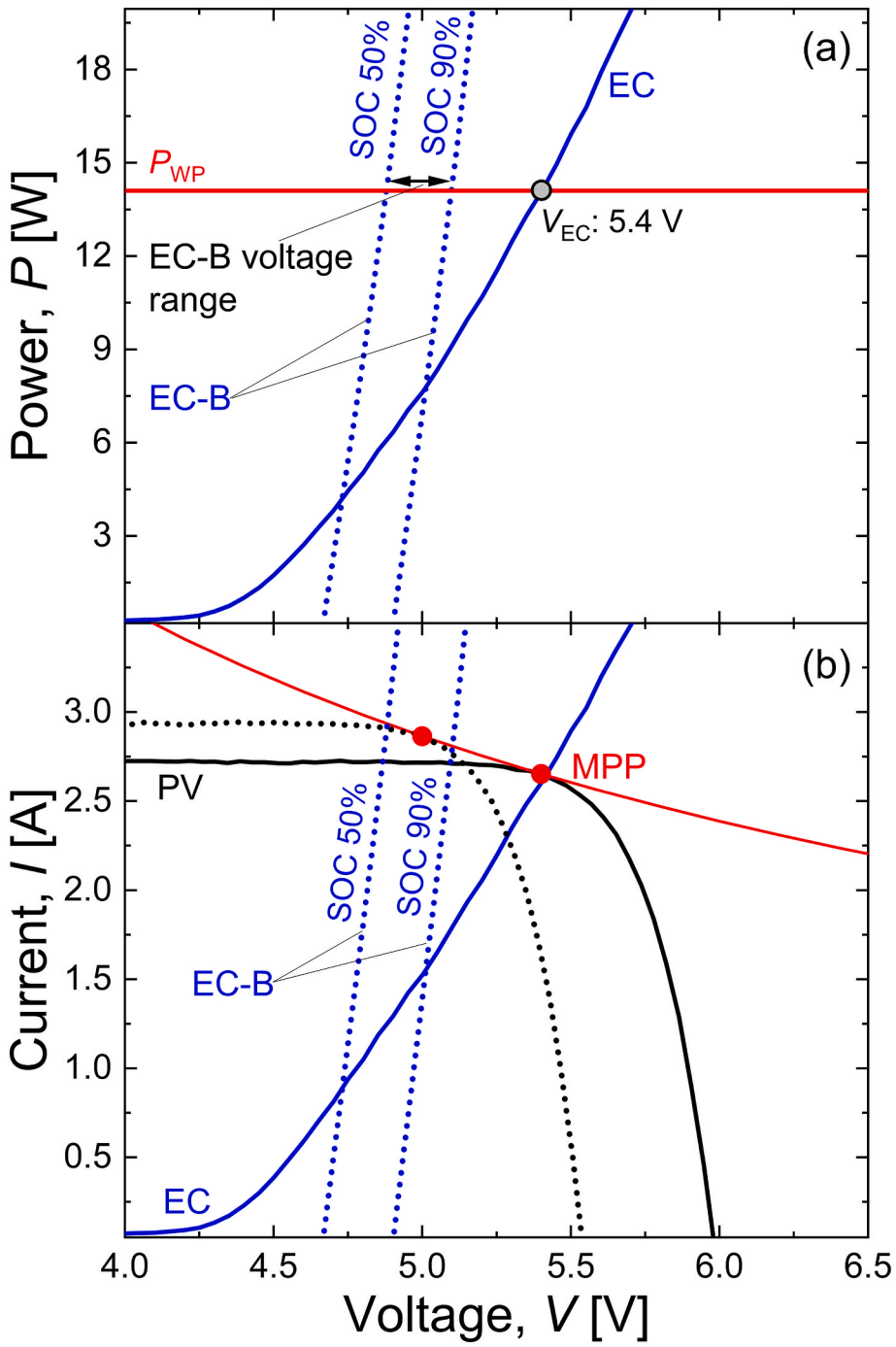

Fig. 2. **(a)** Blue line is the power versus voltage characteristics for the used electrolyzer. Red line indicates the power requirement or working point power P_{WP} to run the electrolyzer at recommended voltage. Blue dotted lines are the combined EC and battery power versus voltage characteristics at 50 % and 90 % battery state of charge (SOC). **(b)** Red line is the MPP trace for GaAs PV module for the power requirement of the electrolyzer using solar concentration of 17.3 suns and a PV efficiency of 34.5 %. Solid black line is the PV *IV* corresponding to maximum coupling for the planned PV-EC experiment. Solid blue line is the EC polarization curve at a scan rate of 50 mV/min. Dotted black line is the PV *IV* corresponding to maximum coupling for the planned PV-EC-B experiment. Dotted blue lines are the combined EC and battery *IV* characteristic at 50 % and 90 % battery SOC, respectively. Red solid circles are the points of maximum coupling for both PV-EC and PV-EC-B experiments. (For interpretation of the references to colour in this figure legend, the reader is referred to the Web version of this article.)

$$GA_{PV}\eta_{PV} = P_{EC} = I_{EC}V_{EC} \tag{5}$$

where G is the solar irradiance, A_{PV} is the PV device area, η_{PV} is the PV power conversion efficiency, P_{EC} the power requirement of the EC element, I_{EC} the EC current and V_{EC} the EC voltage. Once the PV device area is set, we need to determine the number of PV cells N_{cPV} to be connected in series to achieve the required maximum power point voltage as.

$$N_{cPV} = V_{EC}/V_{MPP\ Cell} \tag{6}$$

where $V_{MPP\ Cell}$ is the maximum power point voltage of the characterized PV cell. Commonly, for an electrolyzer stack with an arbitrary number of EC cells N_{cEC}, the EC voltage is a product N_{cEC} and $V_{EC\ Cell}$. The problem can be generalized with a cell ratio C_R, the ratio of PV to EC cells resulting in proper voltage matching via the target operating EC cell

voltage V_{ECcell} and PV cell MPP voltage V_{MPP}

$$C_R = N_{cPV}/N_{cEC} = V_{EC\ Cell}/V_{MPP\ Cell} \quad (7)$$

Note that any practical size system with more than one EC cell and one PV cell can result in fractional C_R, for optimal coupling [58]. In practical applications, the required number of the components is achieved by an interconnection of cells of different size and number which allows smooth tuning of both current and voltage to achieve proper power coupling [21,25,46,59–66]. However, the lab scale experiments are severely constrained in the fine tuning of coupling due to the small number of cells involved in the system and subsequently very coarse voltage steps. In this work we overcome this limitation by using hardware PV emulator – an SMU controlled by a dedicated software reproducing any required PV *IV* characteristics with accuracy and precision on par with AAA Class solar simulator [67]. Note that the PV emulation reproduces *IV* and emulates direct coupling to PV module without MPPT tracking. This approach provides necessary flexibility in planning and reproducibility in conducting of the experiment. So, we can reproduce the operation of a PV module with fractional number of cells when one or only few EC cells are available for laboratory testing. For example, if the target operating voltage of the water splitting cell is 1.8V and the maximum power point voltage of a PV cell is 0.5V the optimal coupling is achieved in practice when a stack of 5 EC cells is connected to a PV module of 18 PV cells. This yields a C_R of 3.6. To realize these conditions for a single EC cell we can take a single PV cell *IV*, multiply its voltage scale values by the C_R to achieve the emulated *IV* voltage V_{ePV}:

$$V_{ePV} = V_{PV}C_R \quad (8)$$

At the same time, we must divide the current values of the original PV *IV* characteristic by C_R to ensure operating at the same target PV power and area. Therefore, for the PV device with JV characteristics $J_{PV}(V_{PV})$, where J is current density and the required PV area A_{PV}, the emulated *IV* current I_{ePV} is given by

$$I_{ePV} = J_{PV}A_{PV}/C_R \quad (9)$$

The resulting dataset $I_{ePV}(V_{ePV})$ is loaded into the emulator program and the required operating conditions are achieved at the lab scale with a single or few cells EC device. The resulting black solid PV line in Fig. 2 (b) represents the emulated $I_{ePV}(V_{ePV})$ used in the PV-EC experiment.

The constant PV power reciprocal red line shown in Fig. 2 (b) was calculated according to the PV efficiency η_{PV} equation [25,43,66,68].

$$\eta_{PV} = P_{MPP}/GA_{PV} = I_{MPP}\ V_{MPP}/GA_{PV} \quad (10)$$

making $I_{MPP} = 14.3\ W/V_{MPP}$ for the required PV power of 14.3 W and represents a GaAs type PV device with $\eta_{PV} = 34.5$ %, under concentrated light with $G = 17.3$ suns (17.3 kW/m^2) and $A_{PV} = 415.2$ cm^2.

The key idea of the first experiment is to compare the reference PV-EC system to the equivalent PV-EC-B system in the same working cycle and isolate the effect of the battery on the solar-to-hydrogen efficiency. To ensure that the difference in the performance is solely related to the battery, both the PV-EC and the PV-EC-B systems must have same, ideally maximal coupling factor. In directly connected systems this requirement is not automatically fulfilled when the same PV and EC devices are measured with and without battery, because the battery shifts the operating point of the device and thereby affects the coupling [43,44], which makes direct comparison of PV-EC and PV-EC-B systems challenging at the highest efficiency level. In our previous experimental work [44], we overcame this comparison issue by designing the experiment in such a way that the operating voltage was above the PV MPP in the PV-EC system, while the battery shifted the operating voltage below the PV MPP in the PV-EC-B system. Both systems had the same degree of coupling loss with C ≈ 0.93 which allowed to isolate the synergistic effect of the battery on the STH efficiency.

The aim of the current study is to determine the STH gain achieved with a battery in a well optimized system with high efficient components. Therefore, in the present study we design both PV-EC and PV-EC-B systems to have optimal coupling with coupling factor as close to unity as possible by using the hardware PV emulator. Therefore, when the battery is connected in parallel to the electrolyzer, the coupling in the system has to be reoptimized in order to ensure that the $I_{ePV}(V_{ePV})$ characteristic of the PV device match the common *IV* characteristics of the battery and EC systems [43,44]. Both EC and battery are connected in parallel to PV and their common load *IV* is the sum of their currents at each voltage point. The battery *IV* for the typical working range of charge/discharge currents is well approximated by a steep line crossing the voltage axis at the battery open circuit voltage. This voltage depends on the state of charge (SOC), while the slope of the line is defined by the internal battery resistance [42]. Experimental battery *IV*s can be determined by taking current-voltage pairs from the family of charge-discharge curves [33]. In our study, we cover SOCs between 50 % and 90 %, and the corresponding battery *IV*s are shown in Supplementary_doc1 Fig. S3. In a properly scaled PV-EC-B system, the battery *IV*s are much steeper than the EC *IV*s, so the resulting sum curve is dominated by the battery [43,44]. The intersection of the PV *IV* and the common EC-B IV determines the operating point of the PV-EC-B system. These EC-B characteristics are shown in Fig. 2. The EC-B combined power curves are presented with dotted blue lines in Fig. 2 (a) for two battery states of charge of 50 % and 90 %, respectively. To obtain the new $I_{ePV}(V_{ePV})$ curve that is optimally matched to EC-B combination, we follow the same procedure as described above for the identical PV cell and PV area. The resulting $I_{ePV}(V_{ePV})$ curve is presented as dotted black line in Fig. 2 (b) with $I_{MPP} = 2.86$ A, $V_{MPP} = 5.00$ V, and C_R of 0.65. As a target voltage, we choose 5 V which is the midpoint between the medium and high battery SOC. Note that the PV *IV* characteristic in the case of the PV-EC-B system (dotted black line) has it's MPP at a lower voltage compared to the MPP for the PV-EC system (solid black line) despite the maximum PV power being the same in both cases. This difference in MPP is the direct consequence of the power splitting between battery and EC cells during the daytime which is expected to lead to a reduction of the kinetic, ohmic etc. losses in the EC process. The sets of coupling parameters for both PV-EC and PV-EC-B systems are designed to isolate the effect of the battery in an idealized operating cycle. Optimal coupling for realistic application scenarios will require simulations with site-specific time series of irradiance and temperature over years of operation [46].

2.2. PV modules and PV emulator

A gallium arsenide (GaAs) photovoltaic 1-cell module is characterised and used as the building block for the emulated PV array used in this work. The single-cell PV module with a PV cell area ($A_{PV\ cell}$) of 25 mm^2 is characterised using a class AAA solar simulator under a solar concentration of 17.3 suns. A Fresnel lens is used as the solar concentrator with the module yielding a short circuit current (I_{SC}) of 60 mA, an open circuit voltage (V_{OC}) of 2.84 V, a current at MPP (I_{MPP}) of 58.3 mA, and a voltage at MPP (V_{MPP}) of 2.56 V with an efficiency of 34.5 %. Considering that a solar concentrator (Fresnel lens) is used, the area of PV (A_{PV}) in the context of this work is taking as the area of the solar concentrator ($A_{concentrator}$) as previously expressed in equation (4). Where $A_{PV\ cell}$ is the PV single-cell module area. A_{PV} during characterisation of the 1-cell module therefore has a value of 432.5 mm^2.

In this study, the PV device driving EC and EC-B combinations in the experiment is realized through the hardware emulation. The PV emulator provides high flexibility, reproducibility and temporal stability of the PV part of the system. Most of all, this approach provides flexibility to put EC or EC-B devices in the required scenario when fractional numbers of PV cells or smooth adjustment of the PV area are required as discussed in the section above. The versatility of this approach has resulted in the development of a number of PV emulators [69,70]. As proposed and developed by Seidler et al. [67], the PV emulator in this work is based on a Python and SCPI algorithm that dynamically controls

the output of a source measuring unit (SMU) to reproduce the *IV* characteristic of any required PV device with precision and accuracy on par with that of a class-AAA solar simulator. This method offers reproducibility of PV characteristics using off-the-shelf equipment in typical electrochemical laboratories. Using this principle, the PV *IV* characteristic is tailored to conditions required for ideal coupling as shown with solid black line and dotted black lines for PV-EC and PV-EC-B systems, respectively, in Fig. 2 (b). The area A_{PV} for the PV-EC and the PV-EC-B systems, which is the area of the concentrator, is therefore adjusted to 415.2 cm^2 during emulation to match the power requirements of the EC cell. This yields I_{SC} of 2.73 A, V_{OC} of 5.98 V, I_{MPP} of 2.65 A, V_{MPP} of 5.40 V and efficiency of 34.5 % with C_R of 0.70 for the PV-EC experiment and I_{SC} of 2.95 A, V_{OC} of 5.53 V, I_{MPP} of 2.86 A, V_{MPP} of 5.00 V and efficiency of 34.5 % with C_R of 0.65 for the PV-EC-B experiment, respectively.

2.3. Electrochemical cell

An Electro-MP (Multipurpose) cell from Electrocell Europe in Denmark is used as the electrochemical cell for water splitting in this work. With the ability to stack more than one cell in series, an EC cell stack of 3 cells is operated at 80°C using an acidic electrolyte of 0.5 M H_2SO_4. Each cell in the stack has a platinum-titanium (Pt–Ti) cathode/negative terminal for the hydrogen evolution reaction (HER) and a ruthenium-iridium (Ru–Ir) anode/positive terminal for the oxygen evolution reaction (OER). The HER and OER chambers are separated by a Nafion membrane to prevent gas mixing within the EC cell. The image of the EC cell components for a single cell is shown in Supplementary_doc1 Fig. S1. The active area of each electrode is 100 cm^2, giving a total EC cell area of 300 cm^2 for the stack of 3 cells. The polarization curve at a scan rate of 50 mV/min for the EC cell stack is shown as the solid blue curve in Fig. 2 (b). Note that each cell in the EC cell stack operates at 1/3 of the voltage shown in the polarization curve, as the cell voltages add up when the cells are connected in series. The flow rate of the electrolyte through the EC is maintained at 300 ml/min using a peristaltic pump. Using a water-gas displacement, the faradaic efficiency of the EC is analyzed to be approximated to 100 % for the relevant range of current utilized by the EC cell stack and presented in Supplementary_doc1 Fig. S2.

2.4. Batteries

Two commercially available lithium titanium oxide (LTO) batteries connected in series are used. Each battery has a nominal voltage of 2.4 V and nominal capacity of 6 Ah. An image of one battery is shown in Supplementary_doc1 Fig. S1. The charge-discharge curves for the battery at different charge-discharge rates/currents are shown in Supplementary_doc1 Fig. S3. From the charge discharge curves, the battery *IV*s can be obtained for different SOC. The *IV* for the combination of the EC and batteries are therefore shown with dotted blue lines in Fig. 2 (b) at 50 % and 90 % battery state of charge (SOC).

2.5. Experimental procedure/duty cycle

The PV-EC experiment is conducted using PV emulation, whereby the PV characteristics illustrated by the solid black line in Fig. 2 (b) are emulated for a 2-h illumination period. The electrolyte flow rate is maintained at 300 ml/min and at 80 °C. During this operational phase, a Keithley 2651 A source measuring unit (SMU) is employed to emulate the output of the PV, thereby providing readings for the PV voltage and current. Furthermore, a Keithley digital multimeter (DMM) is employed to concurrently ascertain the voltage of the EC cell stack.

The experiment is conducted for the PV-EC-B configuration by connecting two series-connected LTO batteries in parallel to the previously established PV-EC system. The PV output characteristics for PV *IV*, as illustrated by the dotted black line in Fig. 2 (b), are then replicated for the same illumination period as the PV-EC experiment (i.e., 2 h). Furthermore, additional digital multimeter (DMM) devices are employed to ascertain the voltage of the battery, and the voltage drop across a 1 mΩ sense resistor to evaluate the current received by the battery. Following the 2-h illumination period, the PV emulator output is turned off, with an additional 4-h run time permitted to facilitate the discharge of the battery by the EC cells resulting to a total of approximately 6 h for the PV-EC-B experiment.

Subsequently, additional measurement in PV-EC configuration with downscaled PV is conducted for 2 h. The relative scaling of the electrolyzer can be described via the area ratio A_R defined as the ratio of PV area A_{PV} to the EC area A_{EC}

$$A_R = A_{PV}/A_{EC} \tag{11}$$

This area ratio can be thought of as the power concentration ratio, i.e. higher A_R results in higher EC power density. If a PV-EC system optimized for a certain EC power density is equipped with a battery, the EC power density decreases as the battery distributes energy over time. This allows to increase A_R, i.e. reduce electrolyzer capacity per unit PV area. We seek to experimentally determine the extent to which A_R can be increased in PV-EC-B system while maintaining the same STH efficiency as the PV-EC system. In our experimental setup, to ensure constant performance and direct comparison between experiments, the electrolyzer itself was not resized or modified. Instead, the area ratio is modified by changing the PV area, which can be flexibly changed utilizing the PV emulator. That is; to observe the effect of increased area ratio in PV-EC-B system, we performed another reference experiment measuring PV-EC system with lower A_R. The difference in A_R of this new reference PV-EC system and the already measured PV-EC-B system shows how far the electrolyzer can be scaled down in system with battery at same STH efficiency level. In the preparation for the experiment we identified that reduction of PV area by factor 2 in the new PV-EC system satisfies the conditions. Therefore, the new reference PV-EC experiments were performed at $A_R = 0.7$ and compared to the already measured PV-EC and PV-EC-B systems with $A_R = 1.4$.

3. Results

3.1. System operation in idealized cycle

The system parameters for the PV-EC system and the PV-EC-B system are presented in Fig. 3. The parameters pertaining to the PV-EC system are presented in green on the left side of the figure, while the parameters pertaining to the PV-EC-B system are presented on the right side. The duration of the PV-EC experiment is 2 h. In contrast, the duration of the PV-EC-B experiment is approximately 6 h, consisting of 2 h of illumination and approximately 4 h of night/dark operation during which the battery powers the EC cell stack.

Fig. 3(a) illustrates the voltage in both systems during the experimental cycle. For the PV-EC system (left side), the PV voltage (V_{PV}) is nearly constant at approximately 5.49 V for an illumination period of 2 h following an initial slight increase. V_{PV} during the experiment is recorded to be approximately equal to the voltage of the EC system (V_{EC}) showing no significant voltage drop across the electrical cables. The voltages in the PV-EC-B system are shown on the right side of Fig. 3 (a). PV output voltage V_{PV} is shown with red line which increases from 4.75 V to 5.18 V during the illumination time of 2 h. The voltages of the electrochemical cell (V_{EC}) and the battery (V_B) shown with black and blue lines also follow V_{PV} during the illumination time. The shift in voltage during illumination for the PV-EC-B system is related to the increase in voltage of the battery as it is charged. During the dark period, the PV device is idle, and EC cell stack is driven by the battery with V_{EC} following V_B which decreases from 5.18 V to 4.7 V as the battery discharges through the EC cells. Throughout the whole cycle, the PV-EC-B system operates at lower voltages than the PV-EC system converting same amount of PV energy.

The currents (*I*) in the PV-EC and PV-EC-B systems are shown in

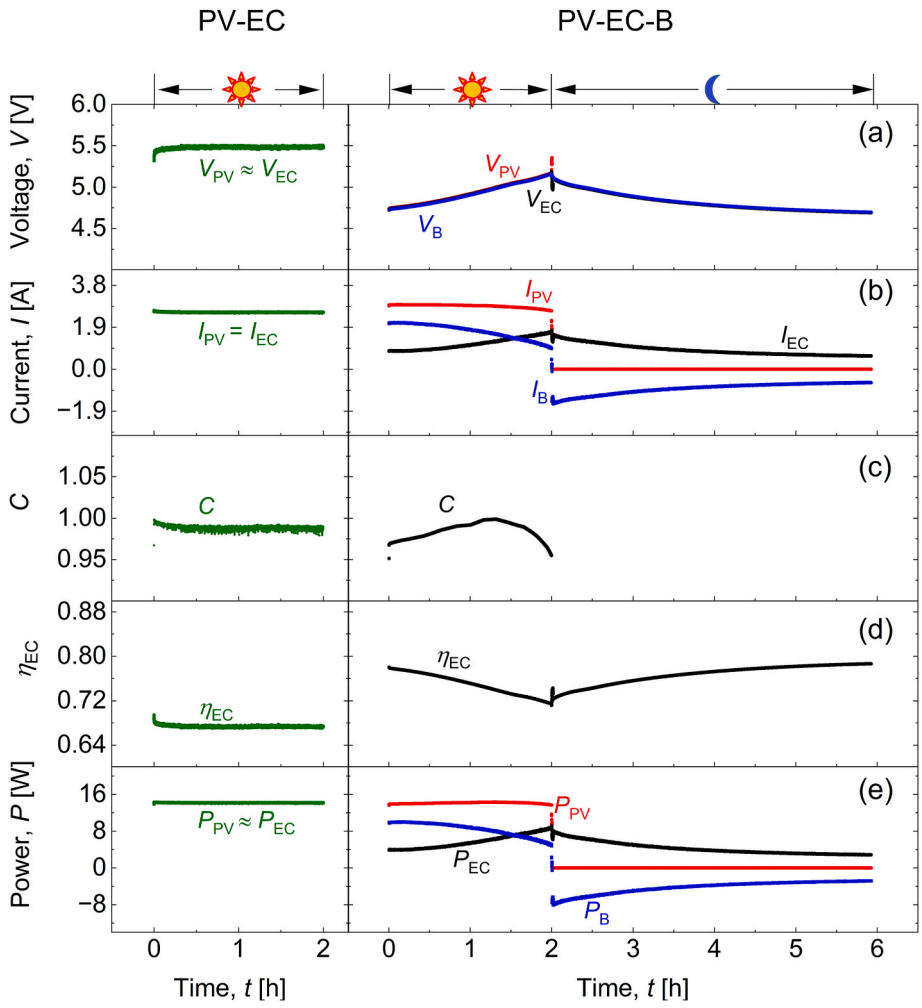

Fig. 3. System parameters for PV-EC experiments on the left side (green) and PV-EC-B experiments (red – black – blue) on the right side. **(a).** Plot of voltage versus time. V_{PV} is the PV voltage, V_{EC} is the EC voltage and V_B is the battery voltage. **(b).** Plot of current versus time. I_{PV} is the PV current, I_{EC} is the EC current and I_B is the battery current. **(c).** Coupling factor versus time. C is the coupling factor **(d).** EC efficiency versus time. η_{EC} is the EC efficiency **(e).** Power versus time. P_{PV} is the PV power, P_{EC} is the EC power and P_B is the battery power. (For interpretation of the references to colour in this figure legend, the reader is referred to the Web version of this article.)

Fig. 3 (b). For the PV-EC system, the PV current (I_{PV}) shown as green trace is equal to the current received by the EC cell stack (I_{EC}) and stays constant at 2.56 A for the illumination time of 2 h. For the PV-EC-B experiment, I_{PV} is plotted with red line and shows a value of approximately 2.95 A at the onset of the illumination period, declining to approximately 2.68 A at the end of the illumination period. This behaviour illustrates a decrease in PV current as the working point of the PV device shifts towards higher voltages exceeding V_{MPP} at the "knee" of the PV *IV* characteristic. In PV-EC-B system I_{PV} is split between the current of the EC cell stack (I_{EC})-black line and the current of the battery (I_B)-blue line in Fig. 3(b). At the onset of the illumination period, at low battery SOC, its voltage is low and more current flows to the battery than to the EC cell stack. With charging and increase of SOC, the battery voltage increases and the current distribution shifts towards the electrolyzer. In the dark, the PV current is absent, and EC cell stack is supplied by the battery. The battery current changes polarity as battery switches from charge to discharge mode. During this period, the EC current declines slowly as the battery discharges and its voltage decreases.

The coupling factors (C) for both PV-EC and PV-EC-B experiments are shown in Fig. 3 (c). The green plot shows C for PV-EC experiment which shows a constant value of about 0.98 after a slight decrease at the onset of the illumination period as the system's voltage moves away from V_{MPP}. However, after the stable voltage is achieved, the system maintains a fairly constant C. In comparison to the PV-EC-B system (black trace), C increases to from 0.96 to 1 and then drops to about 0.95. This change is because of the significant shift in the system's voltage as the battery is charged. However, both the PV-EC system and the PV-EC-B system maintain significantly high C with values above 0.95 that are representative for direct comparison of their efficiencies.

The EC efficiency (η_{EC}) is shown in Fig. 3 (d). The η_{EC} is calculated using equation (12) expressed as the product of voltage efficiency (η_V) and faradaic efficiency (η_F) of the EC cell stack.

$$\eta_{EC} = \eta_V \ \eta_F \tag{12}$$

The voltage efficiency is calculated as the ratio of the minimum voltage required for water splitting ($E^\circ = 1.23$ V) [71–73] to the actual operating voltage of the EC system. Considering the fact that there are 3 cells in the EC stack connected in series, the voltage efficiency is therefore calculated using equation (13) where E° is multiplied by the number of EC cells in series N_{cEC}. With an approximation of the η_F to be equal to 100 %, η_{EC} is therefore equal to η_V.

$$\eta_{EC} = \eta_V = N_{cEC} E^o / V_{EC} \tag{13}$$

The EC efficiencies η_{EC} for the PV-EC (green plot) and PV-EC-B (black plot) in Fig. 3 (d) follow therefore an inverse trend for the V_{EC}. The PV-

EC system shows a lesser η_{EC} of about 0.67 giving the generally higher operating voltage of the PV-EC system in comparison to the PV-EC-B system. The η_{EC} for the PV-EC-B system has a decreasing trend from 0.78 to 0.71 during the illumination time giving the increase in voltage of the battery which shifts the system to higher voltages. In the dark, the system has an increasing trend for the η_{EC} from 0.73 to 0.79 as the battery discharges to lower voltages. This trend is a synergistic effect between the battery and EC cell stack since the battery roundtrip potential loss is subtracted from the EC potential loss and therefore is essentially cancelled [43,44]. In other words, independently on the route taken by the charge (i.e., whether during illumination from the PV module directly to the EC cell or during the dark from the battery to the EC cell), it originates from PV potential and arrives at the reference potential E°. Therefore, as long as the charge is delivered to the EC cell, the voltage loss in the battery is irrelevant.

The power profiles of the PV-EC and PV-EC-B systems are shown in Fig. 3 (e). For the PV-EC system, the power of the PV (P_{PV}) – green plot is approximately equal to the power received by the EC (P_{EC}) given that there is a minimal voltage drop across the connecting cables. Both PV-EC and PV-EC-B systems operate close to the same PV P_{MPP} of 14.3 W. For the PV-EC-B system, P_{PV} (red plot) is split between P_{EC} (black plot), and the battery power (P_B) (blue plot), during the illumination time. Similarly to the current profiles, at the start of the illumination period, a greater proportion of the power is directed to the battery than to the EC cell stack, as the battery charges from a lower SOC to a higher SOC. As the illumination period continues, the EC cell stack begins to receive a greater proportion of the power, as the battery reaches its maximum charge. In the absence of solar input, the P_{PV} is zero, with the battery transferring its power to the EC cell stack. During this dark period, the battery's power output declines to lower voltages and the working point shifts to lower EC currents.

The system parameters demonstrate that despite both systems being subjected to the same input solar power P_{PV}, the power distribution and utilization towards the production of hydrogen are different. In the system with battery, the EC cell has been consistently powered over the whole cycle. This continuity is achieved without any power electronics by utilizing the basic operation features of the three system elements confirming the conclusions of the previous studies [43,44]. In contrast to the PV-EC system, the same PV energy is utilized at significantly lower EC power in the system with battery. Therefore, throughout the cycle, the EC system operates at lower voltages and lower overpotentials in the PV-EC-B case. In the next section we analyse the energetic implications of this battery effect.

3.2. Synergistic STH gain using battery

In order to characterize the STH efficiency in the PV-EC-B system, the total energy over the cycle has to be considered. To compare both systems, we integrate power over the experiment time as shown in Fig. 4(a) and (b).

In Fig. 4 (a) and (b) the blue line represents the energy of the PV device at MPP (E_{MPP}) according to equation (14) as the integral of the power at MPP (P_{MPP}) with respect to time. All integrals were calculated from the dataset using rectangle rule. E_{MPP} represents the energy that would be generated by the PV device assuming continuous operation at its MPP, i.e. the maximum energy extractable from the PV device over the illumination period.

$$E_{MPP} = \int P_{MPP}.dt \tag{14}$$

E_{MPP} (blue line) increases linearly from the onset of the illumination time for the PV-EC and PV-EC-B systems, reaching a maximum value of 28.7 Wh after 2 h which is the end of the illumination time for both systems. Both systems exhibit the same E_{MPP} as the PV devices has the same maximum power. For the PV-EC-B system, E_{MPP} remains flat/constant after 2 h as there is no solar energy input to the system anymore.

E_{PV} represents the actual working point energy of the PV for both the PV-EC and PV-EC-B experiments, as illustrated by the red line in Fig. 4 (a) and (b), respectively. It corresponds to the integral of the actual power of the PV device with respect to time:

$$E_{PV} = \int P_{PV}.dt \tag{15}$$

E_{PV} (red line) increases linearly from the onset of the illumination for both systems to a maximum value slightly less than E_{MPP} after 2 h. The final difference between E_{MPP} and E_{PV} gives the energy loss due to coupling. This yields an energy loss to coupling of 1.15 % and 1.58 % for the PV-EC and PV-EC-B systems, respectively. Consequently, the coupling efficiencies (η_C) of the PV-EC and PV-EC-B system yields values of 98.9 % and 98.4 %, respectively. These overall high values demonstrate the possibility of the directly coupled systems to function with high degree of coupling without power electronics for MPP tracking and aids for the comparison of efficiencies of both systems.

Fig. 4(a) and (b) illustrate the energy received by the EC cell stack (E_{EC}), represented by the black line which is defined as the integration of the power received by the EC cell stack with respect to time:

$$E_{EC} = \int P_{EC}.dt \tag{16}$$

In the case of the PV-EC experiment, the trend observed in E_{EC} is consistent with that of E_{PV}, reflecting the instantaneous transfer of energy from the PV to the EC system over the illumination period. In the case of the PV-EC-B system, E_{EC} increases in line with the magnitude of the energy transfer to the EC cell stack, given that the energy from the PV device is divided between the EC system and the battery. Consequently, E_{EC}, even after the illumination period for the PV-EC-B system, continues to rise to a value that is approximately equal to the final value of E_{PV}, as the energy from the battery is transferred to the EC cell stack. The difference between E_{PV} and E_{EC} for both systems give the energy loss to wiring/contact resistances. This yields an energy loss to wiring of 0.08 % and 0.83 % for the PV-EC and PV-EC-B systems, respectively. A higher wire loss is experienced in the PV-EC-B system giving the use of additional cables to connect the batteries to the system. Consequently, the wiring efficiencies (η_W) of the PV-EC and PV-EC-B system yields values of 99.9 % and 99.2 % respectively.

The energy of the battery is represented with the orange line in Fig. 4 (b) for the PV-EC-B system and determined by the integration of the power of the battery with respect to time:

$$E_B = \int P_B.dt \tag{17}$$

Since the energy of the PV device during illumination is split between the EC system and the battery, the energy of the battery rises with the proportion of the energy of the PV device it receives. After 2 h, which is the end of the illumination period, the battery gets to a peak value of 16.7 Wh which begins to decrease in the absence of solar power as the battery transfers this energy to the EC system. At the end of the dark period, the battery is depleted and the overall cycle of energy transfer from the PV system to the EC system finished.

The energy of produced hydrogen for both systems denoted as E_{H2} is plotted with green in Fig. 4(a) and (b). The hydrogen energy is given by the integral of the product of the EC current, I_{EC} and $E^\circ = 1.23$ V with respect to time:

$$E_{H2} = \int I_{EC}\ N_{cEC}\ E^o.dt \tag{18}$$

For the PV-EC system, E_{H2} increases linearly as the current of the EC cell is fairly constant. For the PV-EC-B system, the development of E_{H2} is affected by the magnitude of current flowing to the EC cell stack. The final difference between the energy of the EC cell stack E_{EC}, and energy

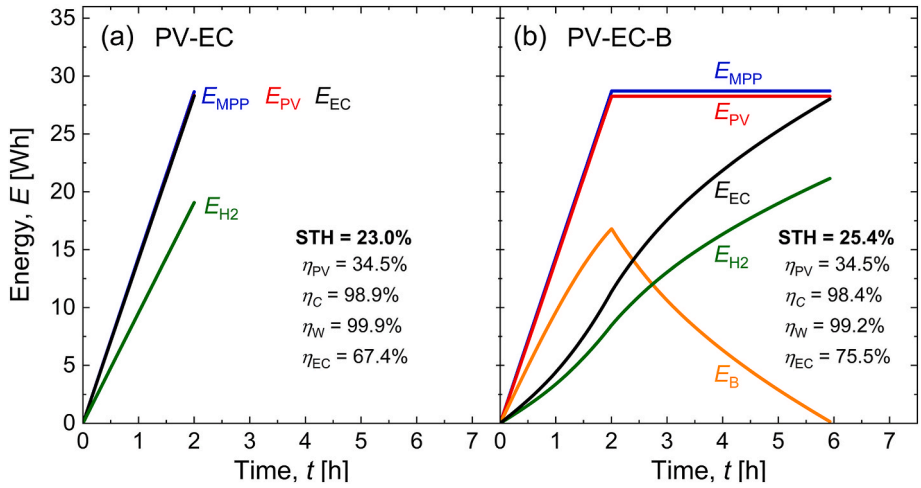

Fig. 4. (a). Energy profiles for PV-EC experiment. E_{MPP} is the PV energy at maximum power point. E_{PV} is the actual energy of the PV device during the experiment. E_{EC} is the energy received by the electrochemical cell/electrolyzer during the experiment. E_{H2} is the energy of produced hydrogen during the experiment. STH is the solar-to-hydrogen efficiency, η_{PV} is the PV efficiency, η_C is the coupling efficiency, η_W is the wiring efficiency and η_{EC} is the EC efficiency. **(b).** Energy profiles for PV-EC-B experiment. All notations retain original meanings as in (a) with E_B representing the energy of the battery.

of hydrogen E_{H2} determines the energy loss in the EC cell stack. This yields an EC efficiency (η_{EC}) of 67.4 % and 75.5 % for the PV-EC and PV-EC-B systems, respectively, given as the ratio of E_{H2} to E_{EC}. The EC cell stack therefore operates at a significantly higher EC efficiency for the PV-EC-B system in comparison to the PV-EC system. This enhanced efficiency is mainly because of the lower operating voltage of the EC throughout the operating cycle for the PV-EC-B system.

The values of STH efficiency for both systems from the energy profiles are calculated as the ratio of the final E_{H2} to the input solar energy E_{in}:

$$\mathrm{STH} = E_{H2}/E_{in} \tag{19}$$

The input solar energy E_{in} is given by the integration of the power received by the PV area for the illumination time T_1

$$E_{in} = \int_0^{T_1} GA_{PV}\, .dt \tag{20}$$

Equation (19) therefore yields a STH efficiency for the PV-EC and PV-EC-B system as 23.0 % and 25.4 % respectively. The results show a total increase of STH efficiency by 2.4 % absolute from the PV-EC to PV-EC-B system as also highlighted in Fig. 4(a) and (b).

The PV-EC system studied in this work with nearly perfect coupling is operating very close to the efficiency limit achievable with the specific set of elements. The limit of the STH efficiency the chosen electrolyzer can achieve with a PV device of any efficiency can be estimated by reverse analysis of its polarization curve according to the method presented in previous studies [51]. The limit is calculated as the dependence of the STH efficiency on the PV efficiency in a PV-EC system with ideal coupling:

$$STH_{limit} = \eta_{PV}\, \eta_{EC} \tag{21}$$

This relation yields the following expression for the STH efficiency limit analysis

$$STH_{limit} = \frac{I_{EC} V_{EC}}{P_{in}}\, \eta_{EC} \tag{22}$$

Hereby η_{EC} is considered the maximum efficiency of the EC system on each point of its polarization curve. A plot to yield the STH limit can therefore be obtained for any EC cell polarization curve.

Considering the obtained experimental results, the STH limit for the PV-EC experiments corresponding to the polarization curve of the EC cell stack and the solar energy input power is presented with red line in

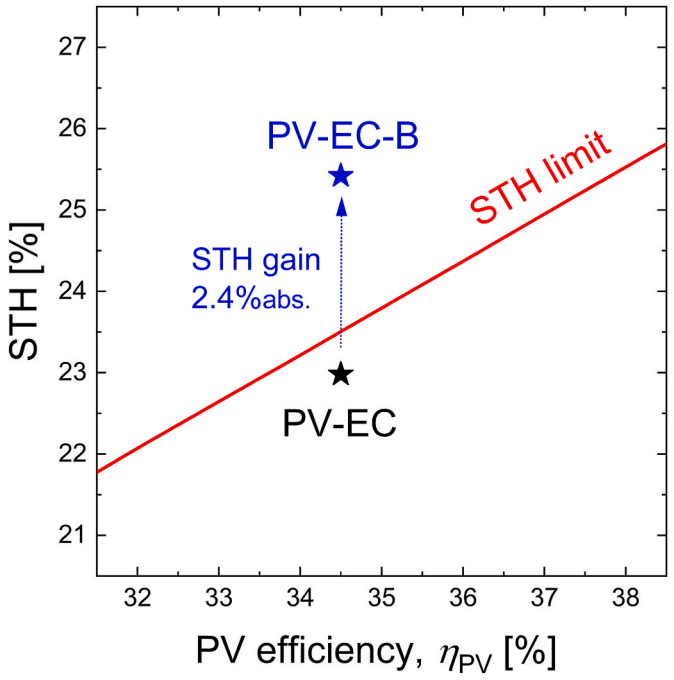

Fig. 5. Solar-to-hydrogen efficiency versus PV efficiency showing the STH limit line in red for PV-EC experiment. Black star represents the PV-EC STH obtained during the experiment while blue star represents the STH for PV-EC-B obtained which is above the STH Limit for the PV-EC configuration. (For interpretation of the references to colour in this figure legend, the reader is referred to the Web version of this article.)

Fig. 5. The black star in Fig. 5 represents the experimentally obtained STH efficiency of the PV-EC system of 23.0 % at a PV efficiency of 34.5 %. The vertical offset between the STH limit and the black star indicates the obtainable STH limit if the PV-EC system functions with optimal coupling of the PV efficiency value of 34.5 %. The experimentally achieved value of 23.0 % is only 0.5 % absolute lower than the STH limit of 23.5 %. These numbers indicate highly optimized system performance. As a comparison, the blue star represents STH value of 25.4 % obtained using a battery in the PV-EC-B system. This value is 2.4 % absolute above the reference value for PV-EC system and 1.9 % absolute above the STH

limit for the PV-EC system. These values illustrate that including a battery in the PV-EC-B system has the possibility of yielding STH values which cannot be achieved in the PV-EC configuration alone in the same operating cycle. The result demonstrates that a properly matched battery included into a PV-EC system is capable to break the intrinsic limit of its STH efficiency.

3.3. EC downscaling potential

The enhanced stability and efficiency of the PV-EC-B system can be utilized to extend the life cycle of the electrolyzer and to enhance hydrogen production. At the same time, relaxed EC cell operation conditions open an opportunity to downscale this costly element and counterbalance the investments related to battery installation. In the second set of experiments, we focus on this issue. From the data of the first set of experiment and previous studies we gained the knowledge that the battery can effectively reduce the EC power by a factor of approximately two. Therefore, we hypothesize that a reduction of the electrolyzer size by the same factor is plausible implementing the battery in the circuit. The EC cell size issue in a general way can be addressed via the area ratio A_R expressed in equation (11) as the ratio of A_{PV} to the A_{EC}.

To evaluate the relationship between the EC area (A_{EC}), the PV area (A_{PV}), and the STH efficiency, a new reference PV-EC experiment was conducted to yield similar STH values as those obtained in the previously discussed PV-EC-B experiment, while comparing the area ratios in both configurations. This approach resulted in an area ratio of 0.7 (A_{PV} = 207.6 cm^2, and A_{EC} = 300 cm^2) for the reference PV-EC experiment. Fig. 6 illustrates the PV *IV* characteristic with dotted black lines corresponding to the reference PV-EC configuration. The point of intersection between the PV *IV* curve and the EC polarization curve is close to optimal coupling for the specified PV area. The trajectory of the maximum power point (MPP) is illustrated with a dotted red line. In this configuration with A_R = 0.7, the implication is that the EC area is larger than the PV area. For a different area ratio A_R = 1.4 (A_{PV} = 415.2 cm^2, and A_{EC} = 300 cm^2), the solid black line in Fig. 6 represents the PV *IV* characteristic required for a maximum coupling in the PV-EC configuration. In this configuration, the EC area is smaller relative to the PV area even though the actual area of the electrolyzer is the same. The solid red line in Fig. 6 corresponds to the MPP trace at this area ratio which is the same area ratio used for the PV-EC-B experiment.

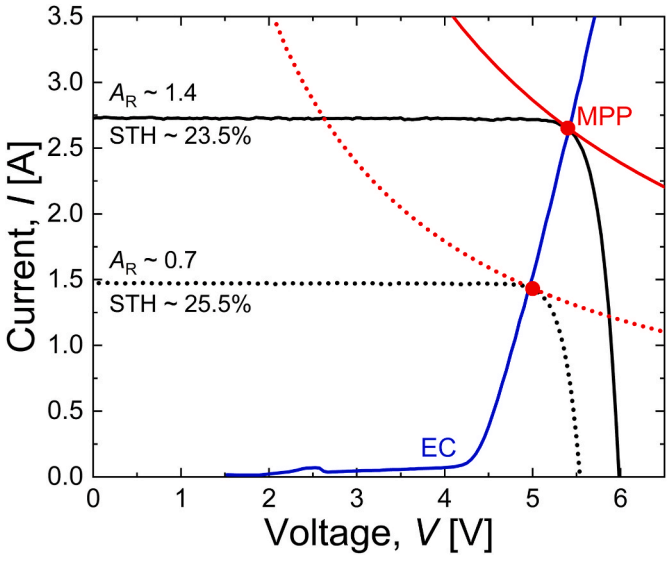

Fig. 6. Blue line is the EC polarization curve. A_R is the PV to EC area ratio given as A_{PV}/A_{EC}. The red dotted line is the MPP trajectory for the GaAs PV module considering an area ratio of 0.7 used as reference, the black dotted line is the PV *IV* characteristic with an area ratio of 0.7, corresponding to the maximum coupling for the planned PV-EC reference experiment. Black solid line is the PV *IV* characteristics corresponding to the maximum coupling for the planned PV-EC experiment with an area ratio of 1.4, red solid line is the MPP trajectory for the GaAs PV module for a solar concentration of 17.3 suns and a PV efficiency of 34.5 % for the area ratio of 1.4. (For interpretation of the references to colour in this figure legend, the reader is referred to the Web version of this article.)

Efficiency and losses in the three measured systems: two PV-EC systems with A_R of 0.7 and 1.4 as well as PV-EC-B system with A_R of 1.4 are presented by the stacked bar diagram in Fig. 7. The red dotted line shows the PV efficiency of 34.5 %. The STH values are presented with the yellow bars, the gray shade shows the coupling loss and the EC loss is shown with blue shade. The system parameters (V_{PV}, I_{PV} etc.) for the smaller A_R of 0.7, are shown in Supplementary_doc1 Fig. S4.

The first bar in Fig. 7 represents the reference PV-EC experiment with an area ratio of 0.7 which demonstrates STH = 25.0 %. After doubling of the area ratio to 1.4 the PV-EC system presented by the second bar in Fig. 7 (V_{PV}, I_{PV} etc. are already presented in Fig. 3 above) shows a reduction of STH by approx. 2 % absolute, down to 23 %. Once the system with the area ratio of 1.4 is reoptimized to accommodate the battery, the full cycle STH efficiency is increased to 25.4 % which is even higher than STH efficiency in the reference system with twice the relative EC capacity. This is a solid indication that application of batteries allows reduction of the electrolyzer capacity by at least a factor of two.

4. Discussion

The first set of experiments in this study is designed to compare the operating characteristics of a PV-EC system and a PV-EC-B system and how batteries are beneficial to improve the STH efficiency. The PV module is directly connected to the other system components (EC cells and batteries) without any power electronics for PV MPP tracking, which demonstrates self-sustenance and potential to eliminate reliability issues or costs related to tracking devices. However, the results are also valid for other coupling modes with DC-DC or DC-AC-DC MPPT etc. solutions.

Using flexibility in PV adjustment, the PV-EC system driven by a PV emulator shows a very high degree of power coupling resulting in STH efficiency of 23.0 % which is only 0.5 % absolute lower than its obtainable STH limit of 23.5 %. The losses are related to minor coupling efficiency fluctuations and nonzero resistive loss in cables in the experimental system. Connecting batteries parallel to the PV-EC system makes it possible to go over this limit with an STH efficiency value of

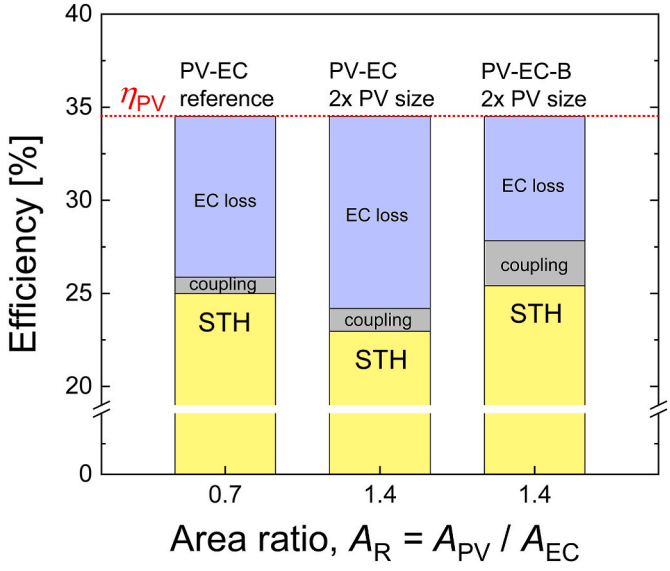

Fig. 7. Efficiencies versus area ratio for the direct coupling experiments performed.

25.4 % achieved for the PV-EC-B system. The EC cell stack and batteries operate synergistically by significantly improving the STH efficiency in comparison to the PV-EC system alone regardless of losses in the battery. The STH gain of 2.4 % absolute or 10 % in relative terms can noticeably increase the hydrogen yield of the system. In our previous work with originally reported STH efficiency gain potential, we anticipated that "… solar-to-hydrogen efficiency gain of 5 %–10 % relative is achievable with properly scaled battery in PV-EC-B system. …" [43]. The nearly perfectly optimized systems in the present work show the experimental STH efficiency gain value corresponding to the top of the anticipated range. In our previous experimental work, less efficient PV and EC devices, in presence of higher coupling losses, achieved STH gain of approx. 9 % relative with battery [44]. Even though the exact value of STH gain depends on the operating cycle [43] we confirm here that batteries can bring STH gain of 5 %–10 %. The absolute gain will therefore depend on the reference efficiency of the PV-EC system. All discussed results are estimated and measured in direct coupled systems but we expect approximately same STH gain in systems coupled via power electronics.

In the original work [43] a method and formula have been suggested for quick estimation of the STH gain that an optimized PV-EC system can achieve in a basic day/night cycle

$$STH_{gain} = \frac{N_{cEC}\, \mathrm{E^o} (I_{\mathrm{PVECB}} - I_{\mathrm{PVEC}})}{P_{in}} \tag{23}$$

where I_{PVECB} is the total daytime current (2.82 A on average) in the optimized PV-EC-B system and I_{PVEC} is the daytime current in the reference PV-EC system (2.56 A). The formula is updated with N_{cEC} to account for the serial connection of the EC cells (3 in this work). The result of the calculation is STH gain of 2.3 % absolute, which is a good estimate of the accurately measured gain of 2.4 % taking the simplicity of the calculation into account.

On the practical side, the boost in STH efficiency even beyond the theoretical limit of PV-EC system, results in hydrogen production gain. We expect the production gain as a preliminary estimate to be of approximately same 10 % relative. Simulation study of grid tied DC-DC coupled PV water splitting system shows potential to gain approximately 40 % in annual hydrogen production with batteries [74]. The 40 % gain is tied to the fact that the power of the PV in this case is about 3 times the nominal capacity of the electrolyzer resulting in excess energy being sent to the grid in the absence of batteries. With the battery some part of the excess energy is used to charge the battery which is used up in the electrolyzer during insufficient irradiance. Therefore, the electrolyzer in the system without the battery experiences lesser PV power while the battery assumes the function of supplying the requisite excess energy for the battery-connected system. At the same time, we demonstrate that in PV-EC-B system the electrolyzer can be downscaled by at least factor two while keeping the STH value of the reference PV-EC system without battery. It is a matter of further technoeconomic and lifecycle assessment which of the effects is more beneficial from environmental and financial viewpoints.

The effect of battery related gain in efficiency and electrolyzer downscaling potential are not specific to the water splitting process. We expect the performance of any PV driven electrolyzer, e.g. for CO_2 reduction, to be improved with battery under natural periodic and intermittent operating conditions.

The constant solar irradiance level utilized in this study is a simplification of typical diurnal irradiance which is chosen to isolate and precisely quantify the effect of the battery. For the same reason, a relatively narrow range of battery capacity has been utilized in the experiment. Future studies must address realistic, upscaled and real outdoor scenarios of irradiance and long-term system operation with stronger utilization of the battery capacity.

High STH values above 20 % are achieved in this work; thanks to the high efficiency concentrator GaAs PV module, with PV efficiency of 34.5 %. The choice is made to study the STH gain at the top level of practically achievable PV efficiencies. The concentrator PV is not the most common technology, and we expect that water splitting electrolyzers will be more likely connected to more typical PV modules without tracking. Nevertheless, recent developments in perovskite-Si tandem solar cells promise to achieve similar results [75,76] without concentrating sunlight, which makes the results from this study achievable with future perovskite-Si tandem PV modules.

5. Conclusions

In this work we study how batteries can stabilize and improve efficiency in PV driven electrolyzer systems. The first system consists of a PV module directly connected to EC cells in a PV-EC configuration. Without batteries connected to the system, an instantaneous transfer of PV power to the EC cells with no dark operation of the EC cells takes place. For the same PV power as with the system without batteries, the second system has a battery pack connected parallel in a PV-EC-B configuration resulting in the splitting of the PV power between the battery and the EC cells. This configuration also allows for dark operation of the EC cells where battery transfers its energy to the EC cells in the dark. Highly efficient components, including concentrated solar irradiance at 17.3 suns for GaAs PV modules with 34.5 % efficiency and an elevated temperature of 80°C for the EC cell operation with industrially relevant electrodes are used. The PV module operation is achieved by emulation ensuring optimized coupling efficiencies for both systems.

High solar-to-hydrogen efficiencies of 23 % and 25.4 % are obtained for the PV-EC and PV-EC-B configurations, respectively. Notably, not only is STH efficiency in PV-EC-B system 2.4 % absolute above the optimized PV-EC reference, but it is 1.9 % absolute above the theoretical STH maximum/limit obtainable from this specific reference PV-EC system. The gain in STH efficiency is synergistic and is achieved despite roundtrip potential losses in the battery. This synergistic effect originates from the distribution of the daily PV energy over longer periods of EC operation i.e. the reduction of the EC input power and the related losses.

In the second part of the work, we study the downscaling potential of the electrolyzer since batteries reduce peak electrolyzer power in the PV-EC-B configuration. We have shown that in PV-EC-B system the electrolyzer can be downscaled by at least a factor of 2 and keep the STH value of the reference PV-EC system without battery.

Both aspects, the increase in STH efficiency and downscaling of the electrolyzer achieved with batteries are not specific to the studied water splitting process. Performance of any PV driven electrolyzer under periodic and intermittent irradiance can be improved. To deeper understand practically achieved gain with battery, future studies must address realistic and real outdoor scenarios of irradiance, as well as long time system operation with stronger utilization of the battery capacity. Finally, the advantages of the batteries must be evaluated in environmental and financial terms via technoeconomic and lifecycle assessment.

CRediT authorship contribution statement

Uchechi Chibuko: Writing – review & editing, Writing – original draft, Visualization, Investigation, Formal analysis, Data curation, Conceptualization. **Tsvetelina Merdzhanova:** Writing – review & editing, Validation, Supervision, Formal analysis, Data curation. **Solomon Agbo:** Writing – review & editing, Formal analysis. **Uwe Rau:** Supervision, Formal analysis. **Ursula Wurstbauer:** Writing – review & editing, Supervision, Formal analysis, Conceptualization. **Oleksandr Astakhov:** Writing – review & editing, Visualization, Supervision, Investigation, Formal analysis, Data curation, Conceptualization.

Data availability

The data supporting this article have been included as part of the Supplementary Information.

Conflicts of interest

The authors declare that they have no know competing financial interests or personal relationships that could have appeared to influence the work reported in this paper.

Acknowledgements

The authors would like to thank Joachim Kirchoff and Daniel Weigand for their technical and laboratory support. Christoph Zahren and Lutz Ruppach are acknowledged for their help with characterisation on of the GaAs concentrator modules. Sergey Shcherbachenko is acknowledged for his support with PV emulation. The authors gratefully acknowledge the European Commission under the DECADE Project (Grant agreements no:862030) as well as the German Federal Ministry of Education and Research, BMBF and the West African Science Service Centre for Climate Change and Adapted Land Use, WASCAL for support in the framework of PV2HBurkina project (DZ004652).

Appendix A. Supplementary data

Supplementary data to this article can be found online at https://doi.org/10.1016/j.ijhydene.2025.04.166.

References

[1] Naqvi SBQ, Singh B. A PV-battery system resilient to weak grid conditions with regulated power injection and grid supportive features. IEEE Trans Sustain Energy 2022;13:1408–19.
[2] Hashemi S, Ostergaard J, Yang G. A scenario-based approach for energy storage capacity determination in LV grids with high PV penetration. IEEE Trans Smart Grid 2014;5:1514–22.
[3] Manimekalai P, Harikumar R, Raghavan S. An overview of batteries for photovoltaic (PV) systems. Int J Comput Appl 2013;82.
[4] Marcos J, Storkël O, Marroyo L, Garcia M, Lorenzo E. Storage requirements for PV power ramp-rate control. Sol Energy 2014;99:28–35.
[5] Chatzigeorgiou NG, Theocharides S, Makrides G, Georghiou GE. A review on battery energy storage systems: applications, developments, and research trends of hybrid installations in the end-user sector. J Energy Storage 2024;86:111192.
[6] Squadrito G, Maggio G, Nicita A. The green hydrogen revolution. Renew Energy 2023;216.
[7] Risco-Bravo A, Varela C, Bartels J, Zondervan E. From green hydrogen to electricity: a review on recent advances, challenges, and opportunities on power-to-hydrogen-to-power systems. Renew Sustain Energy Rev 2024;189.
[8] Zainal BS, Ker PJ, Mohamed H, Ong HC, Fattah IMR, Rahman SMA, et al. Recent advancement and assessment of green hydrogen production technologies. Renew Sustain Energy Rev 2024;189.
[9] Ivanova ME, Peters R, Muller M, Haas S, Seidler MF, Mutschke G, et al. Technological pathways to produce compressed and highly pure hydrogen from solar power. Angew Chem Int Ed Engl 2023;62:e202218850.
[10] Lima GM, Belchior FN, Villena JEN, Domingos JL, Freitas MAV, Hunt JD. Hybrid electrical energy generation from hydropower, solar photovoltaic and hydrogen. Int J Hydrogen Energy 2024;53:602–12.
[11] Gutiérrez-Martín F, Amodio L, Pagano M. Hydrogen production by water electrolysis and off-grid solar PV. Int J Hydrogen Energy 2021;46:29038–48.
[12] Koponen J, Kosonen A, Ruuskanen V, Huoman K, Niemelä M, Ahola J. Control and energy efficiency of PEM water electrolyzers in renewable energy systems. Int J Hydrogen Energy 2017;42:29648–60.
[13] Maclay JD, Brouwer J, Samuelsen GS. Experimental results for hybrid energy storage systems coupled to photovoltaic generation in residential applications. Int J Hydrogen Energy 2011;36:12130–40.
[14] Chen W-H, Hsieh IYL. Techno-economic analysis of lithium-ion battery price reduction considering carbon footprint based on life cycle assessment. J Clean Prod 2023;425.
[15] Ursúa A, San Martín I, Barrios EL, Sanchis P. Stand-alone operation of an alkaline water electrolyser fed by wind and photovoltaic systems. Int J Hydrogen Energy 2013;38:14952–67.
[16] Ursúa A, Barrios EL, Pascual J, San Martín I, Sanchis P. Integration of commercial alkaline water electrolysers with renewable energies: limitations and improvements. Int J Hydrogen Energy 2016;41:12852–61.
[17] Mohammadi A, Mehrpooya M. A comprehensive review on coupling different types of electrolyzer to renewable energy sources. Energy 2018;158:632–55.
[18] Reuß M, Reul J, Grube T, Langemann M, Calnan S, Robinius M, et al. Solar hydrogen production: a bottom-up analysis of different photovoltaic–electrolysis pathways. Sustain Energy Fuels 2019;3:801–13.
[19] Arunachalam M, Han DS. Efficient solar-powered PEM electrolysis for sustainable hydrogen production: an integrated approach. Emergent Materials 2024:1–15.
[20] Gibson TL, Kelly NA. Optimization of solar powered hydrogen production using photovoltaic electrolysis devices. Int J Hydrogen Energy 2008;33:5931–40.
[21] Clarke RE, Giddey S, Ciacchi FT, Badwal SPS, Paul B, Andrews J. Direct coupling of an electrolyser to a solar PV system for generating hydrogen. Int J Hydrogen Energy 2009;34:2531–42.
[22] Maeda T, Ito H, Hasegawa Y, Zhou Z, Ishida M. Study on control method of the stand-alone direct-coupling photovoltaic – water electrolyzer. Int J Hydrogen Energy 2012;37:4819–28.
[23] Brillet J, Yum J-H, Cornuz M, Hisatomi T, Solarska R, Augustynski J, et al. Highly efficient water splitting by a dual-absorber tandem cell. Nat Photonics 2012;6:824–8.
[24] Jia J, Seitz LC, Benck JD, Huo Y, Chen Y, Ng JW, et al. Solar water splitting by photovoltaic-electrolysis with a solar-to-hydrogen efficiency over 30. Nat Commun 2016;7:13237.
[25] Chang WJ, Lee KH, Ha H, Jin K, Kim G, Hwang ST, et al. Design principle and loss engineering for photovoltaic-electrolysis cell system. ACS Omega 2017;2:1009–18.
[26] Kemppainen E, Aschbrenner S, Bao F, Luxa A, Schary C, Bors R, et al. Effect of the ambient conditions on the operation of a large-area integrated photovoltaic-electrolyser. Sustain Energy Fuels 2020;4:4831–47.
[27] Lee M, Ding X, Banerjee S, Krause F, Smirnov V, Astakhov O, et al. Bifunctional CoFeVOx catalyst for solar water splitting by using multijunction and heterojunction silicon solar cells. Advanced Materials Technologies 2020;5.
[28] Park H, Park IJ, Lee MG, Kwon KC, Hong SP, Kim DH, et al. Water splitting exceeding 17 % solar-to-hydrogen conversion efficiency using solution-processed Ni-based electrocatalysts and perovskite/Si tandem solar cell. ACS Appl Mater Interfaces 2019;11:33835–43.
[29] Kakimoto N, Asano R. Linear operation of photovoltaic array with directly connected lithium-ion batteries. IEEE Trans Sustain Energy 2017;8:1647–57.
[30] Li W, Fu H-C, Zhao Y, He J-H, Jin S. 14.1 % efficient monolithically integrated solar flow battery. Chem 2018;4:2644–57.
[31] Paul Ayeng'o S, Axelsen H, Haberschusz D, Sauer DU. A model for direct-coupled PV systems with batteries depending on solar radiation, temperature and number of serial connected PV cells. Sol Energy 2019;183:120–31.
[32] Khouzam KY, Khouzam L. Optimum matching of a photovoltaic array to a storage battery. The Conference Record of the Twenty-Second IEEE Photovoltaic Specialists Conference - 19911991. p. 706-711 vol.1.
[33] Shcherbachenko S, Astakhov O, Chime U, Kin L-C, Ding K, Pieters B, et al. Efficient power coupling in directly connected photovoltaic-battery module. Sol RRL 2023;7:2200857.
[34] Chibuko U, Merdzhanova T, Weigand D, Ezema F, Agbo S, Rau U, et al. Module-level direct coupling in PV-battery power unit under realistic irradiance and load. Sol Energy 2023;249:233–41.
[35] Agbo SN, Merdzhanova T, Yu SC, Tempel H, Kungl H, Eichel RA, et al. Photoelectrochemical application of thin-film silicon triple-junction solar cell in batteries. Phys Status Solidi 2016;213:1926–31.
[36] Agbo SN, Merdzhanova T, Yu SC, Tempel H, Kungl H, Eichel RA, et al. Development towards cell-to-cell monolithic integration of a thin-film solar cell and lithium-ion accumulator. J Power Sources 2016;327:340–4.
[37] Agbo SN, Merdzhanova T, Yu S, Tempel H, Kungl H, Eichel R-A, et al. Photoelectrochemical application of thin-film silicon triple-junction solar cell in batteries. Phys Status Solidi 2016;213:1926–31.
[38] Khouzam KY. Optimum load matching in direct-coupled photovoltaic power systems-application to resistive loads. IEEE Trans Energy Convers 1990;5:265–71.
[39] Khouzam K, Khouzam L, Groumpos P. Optimum matching of ohmic loads to the photovoltaic array. Sol Energy 1991;46:101–8.
[40] Averbukh M, Lineykin S, Kuperman A. Maximum power point matching of solar arrays to arbitrary loads. 2012 IEEE 27th convention of electrical and electronics engineers in Israel. 2012. p. 1–5.
[41] Shi Y, Hsieh T-Y, Hoque MA, Cambarau W, Narbey S, Gimbert-Surinach C, et al. High solar-to-hydrogen conversion efficiency at pH 7 based on a PV-EC cell with an oligomeric molecular anode. ACS Appl Mater Interfaces 2020;12:55856–64.
[42] Astakhov O, Merdzhanova T, Kin L-C, Rau U. From room to roof: how feasible is direct coupling of solar-battery power unit under variable irradiance? Sol Energy 2020;206:732–40.
[43] Astakhov O, Agbo SN, Welter K, Smirnov V, Rau U, Merdzhanova T. Storage batteries in photovoltaic–electrochemical device for solar hydrogen production. J Power Sources 2021;509.
[44] Kin L-C, Astakhov O, Lee M, Haas S, Ding K, Merdzhanova T, et al. Batteries to keep solar-driven water splitting running at night: performance of a directly coupled system. Sol RRL 2022;6:2100916.
[45] Gillessen B, Heinrichs H, Stenzel P, Linssen J. Hybridization strategies of power-to-gas systems and battery storage using renewable energy. Int J Hydrogen Energy 2017;42:13554–67.
[46] Gutiérrez-Martín F, Díaz-López J, Caravaca A, Dos Santos-García A. Modeling and simulation of integrated solar PV-hydrogen systems. Int J Hydrogen Energy 2024;52:995–1006.
[47] Kikuchi Y, Ichikawa T, Sugiyama M, Koyama M. Battery-assisted low-cost hydrogen production from solar energy: rational target setting for future technology systems. Int J Hydrogen Energy 2019;44:1451–65.

[48] Jang D, Kim J, Kim D, Han W-B, Kang S. Techno-economic analysis and Monte Carlo simulation of green hydrogen production technology through various water electrolysis technologies. Energy Convers Manag 2022;258:115499.
[49] Rezaei M, Akimov A, Gray EM. Economics of solar-based hydrogen production: sensitivity to financial and technical factors. Int J Hydrogen Energy 2022;47:27930–43.
[50] Rezaei M, Akimov A, Gray EMA. Levelised cost of dynamic green hydrogen production: a case study for Australia's hydrogen hubs. Appl Energy 2024;370:123645.
[51] Astakhov O, Smirnov V, Rau U, Merdzhanova T. Prediction of limits of solar-to-hydrogen efficiency from polarization curves of the electrochemical cells. Sol RRL 2022;6:2100783.
[52] Astakhov O, Agbo S, Welter K, Smirnov V, Rau U, Merdzhanova T. Storage batteries in photovoltaic–electrochemical device for solar hydrogen production. J Power Sources 2021;509:230367.
[53] Hobold GM, Lopez J, Guo R, Minafra N, Banerjee A, Shirley Meng Y, et al. Moving beyond 99.9 % Coulombic efficiency for lithium anodes in liquid electrolytes. Nat Energy 2021;6:951–60.
[54] Sun S-Y, Zhang X-Q, Yan X-Y, Zhao Z, Zhang Q-K, Huang J-Q. Advances in high-coulombic-efficiency lithium metal anodes under practical conditions in liquid electrolytes. EES Batteries; 2025.
[55] de Groot MT, Kraakman J, Garcia Barros RL. Optimal operating parameters for advanced alkaline water electrolysis. Int J Hydrogen Energy 2022;47:34773–83.
[56] Krishnan S, Koning V, Theodorus de Groot M, de Groot A, Mendoza PG, Junginger M, et al. Present and future cost of alkaline and PEM electrolyser stacks. Int J Hydrogen Energy 2023;48:32313–30.
[57] Kalogirou SA. Solar thermal collectors and applications. Prog Energy Combust Sci 2004;30:231–95.
[58] Patel MT, Khan MR, Alam MA. Thermodynamic limit of solar to fuel conversion for generalized photovoltaic–electrochemical systems. IEEE J Photovoltaics 2018;8:1082–9.
[59] Cerveramarch S, Smotkin E. A photoelectrode array system for hydrogen production from solar water splitting. Int J Hydrogen Energy 1991;16:243–7.
[60] Atlam O, Barbir F, Bezmalinovic D. A method for optimal sizing of an electrolyzer directly connected to a PV module. Int J Hydrogen Energy 2011;36:7012–8.
[61] Sayedin F, Maroufmashat A, Roshandel R, Khavas SS. Optimal design and operation of a photovoltaic–electrolyser system using particle swarm optimisation. Int J Sustain Energy 2014;35:566–82.
[62] Sayedin F, Maroufmashat A, Sattari S, Elkamel A, Fowler M. Optimization of Photovoltaic Electrolyzer Hybrid systems; taking into account the effect of climate conditions. Energy Convers Manag 2016;118:438–49.
[63] Azzolini JA, Tao M, Ayers K, Vacek J. A load-managing photovoltaic system for driving hydrogen production. 2020 47th IEEE photovoltaic specialists conference (PVSC). 2020. p. 1927–32.
[64] Sharifi T, Larsen C, Wang J, Kwong WL, Gracia-Espino E, Mercier G, et al. Toward a low-cost artificial leaf: driving carbon-based and bifunctional catalyst electrodes with solution-processed perovskite photovoltaics. Adv Energy Mater 2016;6.
[65] Bs M, Nadeem MA, Al-Oufi M, Al-Hakami M, Isimjan TT, Idriss H. Sixteen percent solar-to-hydrogen efficiency using a power-matched alkaline electrolyzer and a high concentrated solar cell: effect of operating parameters. ACS Omega 2020;5:10510–8.
[66] Chang WJ, Lee K-H, Ha J-I, Ki Tae N. Hydrogen production via water electrolysis: the benefits of a solar cell-powered process. IEEE Electrification Magazine 2018;6:19–25.
[67] Seidler MF, Pieters B, Zwaygardt W, Haas S, Astakhov O, Merdzhanova T. A photovoltaics emulator for electrochemistry using Python and SCPI. J Power Sources 2025;641:236723.
[68] Astakhov O, Smirnov V, Rau U, Merdzhanova T. Prediction of limits of solar-to-hydrogen efficiency from polarization curves of the electrochemical cells. Sol RRL 2022;6:2100783.
[69] Ram JP, Manghani H, Pillai DS, Babu TS, Miyatake M, Rajasekar N. Analysis on solar PV emulators: a review. Renew Sustain Energy Rev 2018;81:149–60.
[70] Xenophontos A, Rarey J, Trombetta A, Bazzi AM. A flexible low-cost photovoltaic solar panel emulation platform. 2014 power and energy conference at Illinois (PECI). IEEE; 2014. p. 1–6.
[71] Zhang K, Liang X, Wang L, Sun K, Wang Y, Xie Z, et al. Status and perspectives of key materials for PEM electrolyzer. Nano Research Energy 2022;1:e9120032.
[72] Harrison KW, Remick R, Hoskin A, Martin G. Hydrogen production: fundamentals and case study summaries. Golden, CO (United States): National Renewable Energy Lab.(NREL); 2010.
[73] Li W, Tian H, Ma L, Wang Y, Liu X, Gao X. Low-temperature water electrolysis: fundamentals, progress, and new strategies. Materials Advances 2022;3:5598–644.
[74] González del Valle A, García-Linares P, Martí A. Comparative analysis of hydrogen production and economic feasibility: direct versus indirect coupling of photovoltaic systems with electrolyzers. Advanced Energy and Sustainability Research 2024:2400210.
[75] Ying Z, Yang X, Wang X, Ye J. Towards the 10-year milestone of monolithic perovskite/silicon tandem solar cells. Adv Mater 2024;36:2311501.
[76] Xuan J, Shao T, Zang Y, Liu Y, Yan W. Recent developments of charge transporting layers for high-performance monolithic perovskite/silicon tandem solar cells. IEEE J Photovoltaics 2024;15:3–16.